INTERNATIONAL JOURNAL FOR NUMERICAL METHODS IN FLUIDS, VOL. 17, 221–239 (1993)

CALCULATION OF TURBULENT COMBUSTION OF PROPANE IN FURNACES

X. S. BAI AND L. FUCHS

Department of Mechanics/Applied CFD, Royal Institute of Technology, S-100 44 Stockholm, Sweden

SUMMARY

An evaluation of some numerical methods for turbulent reacting flows in furnace-like geometries is carried out. The Reynolds averaged Navier–Stokes equations and the two-equation k–ε model together with either finite-rate or infinite-rate reaction models are solved numerically. Either single- or multiple-step reactions together with the 'eddy dissipation concept' (EDC) are used to model reacting flows with finite reaction rates. The numerical scheme is finite difference based, together with a multi-grid method and a local grid refinement technique. These methods have been used to calculate the combustion of propane in a single- and multiple-burner configurations. In the former case, the sensitivity of the solution to variations in some model parameters (determining the reaction rate) and numerical parameters (mesh spacing) has been studied. It is noted that different dependent variables exhibit different levels of sensitivity to the variation in model parameters. Thus, calibration and validation of models for reacting flows require that one compares the most *sensitive* variables. For engineering purposes, on the other hand, one may calibrate and validate models with respect to the most *relevant* variables. Our conclusion is that since sensitivity of the temperature distribution is relatively mild, one can still use EDC-like methods in engineering applications where details of the temperature field are of minor importance.

KEY WORDS Turbulent reacting flows Modelling Solution sensitivity Numerical methods Multi-grid method Numerical accuracy

1. INTRODUCTION

Detailed analysis of turbulent reacting flows is a necessity for the development of combustion devices, such as the improvement of fuel burning efficiency and pollution reduction. The theoretical analysis of such turbulent combustion processes, which involves turbulences, chemical reactions, atomizations and vaporizations, etc., has been studied for many years.[1–4] In many combustion devices, such as the aircraft gas turbine engines and furnaces, the Reynolds number is large [$Re \approx O(10^6)$], so that the flow is turbulent. In such cases there exists a large variation of scales, from the large scale (of the size of the object) to the small Kolmogorov scale. To resolve the smallest scales a large number of grid points is required, inhibiting the direct simulation of flows with engineering interest. Most often, the averaged properties and the large-scale properties are sought. Often, one uses a two-equation closure model[5–7] to account for the turbulence. This approach has also been adopted in this paper, but it is far from perfect. More recently, other approaches have been tried, such as the Reynolds stress models and large eddy simulations.[8]

The combustion process, such as hydrocarbon oxidation, often contains several hundred steps of elementary reactions. This can be described by a system of Partial Differential Equations (PDEs), in which the number of equations is proportional to the number of elementary reactions.

0271–2091/93/150221–19$14.50

Received 17 November 1992
Revised 23 February 1993

Often, the PDE system is very large and the elementary reactions, as reported in the literature, are not always well understood and can be a source of large error.[9,10] Hence, a fully detailed kinetic mechanism is seldom used for two- or three-dimensional problems. Reduced reaction schemes, such as those employed here, offer a feasible approach for large problems.[11]

A central difficulty in turbulent combustion, where the associated turbulence–chemistry interaction introduces severe additional modelling problems, is caused by the strong non-linearity of the typical reaction rate expressions and the need to evaluate their mean time- (or ensemble-) averaged values.[12,13] The basic approach to this problem is based on modelling the relation between the time scale of turbulent mixing and the chemical reactions. Two such models are the Eddy Break Up (EBU)[14] and the Eddy Dissipation Concept (EDC)[15] models. Compared with other methods, such as the Probability Density Function (PDF) method[16,17] or the flamelet model,[18] the EDC-type models (used also here) are simpler and flexible in applying to 3D complex geometries.

Another important aspect in the numerical computation of turbulent reacting flows is the choice of numerical schemes. Since the number of equations for realistic turbulent reacting flows is large, high numerical efficiency is important for engineering applications. Earlier work mainly utilized SIMPLE-type schemes with point or line relaxations.[19,20] The method is simple; however, the convergence rate of the iteration process is asymptotically slow. Slow convergence becomes a more serious problem when the grid is refined. For numerical efficiency two issues are important: one is how to use a minimal number of iterations to get a predefined error in solving the discrete equations and the other is how to use a minimal number of mesh points to get a required level of accuracy.

One of the aims of this paper is to demonstrate the usage of some advanced numerical methods, e.g. the Multi-Grid method (MG) and local grid refinement techniques, to the simulation of the turbulent reacting flows. The MG method was developed initially for solving elliptic partial differential equations.[21] This method has been applied to the computation of 3D incompressible isothermal flows,[22,23] resulting in a significant improvement in the convergence rate compared to single-grid relaxation methods. For turbulent reacting flows as well as compressible flows, one has to ensure conservation of mass as one changes grids in the MG procedure. Local grid refinements are introduced so that for a given number of nodes nearly maximal accuracy is achieved.[24]

The second aim of this paper is to study the sensitivity of the numerical solution to some model parameters. Here, we use both an infinite-reaction-rate model as well as single- and multiple-step finite-rate-reaction models to study a single-burner configuration, where fuel (propane) and air enter the combustor in different streams. The sensitivity of some of the dependent variables to the selected model and the particular choice of the EDC parameters have been studied. It has been found that the sensitivity is different for different variables. A consequence of this finding would imply that model constants should be calibrated for different cases. The diffusion-flame (infinite-rate) model has also been applied to a gas fired furnace having multiple (six) such burners. These different cases are also aimed at illustrating the properties and the implementations of the methods that we use.

2. GOVERNING EQUATIONS FOR TURBULENT REACTING FLOWS

Turbulent reacting flows can be described by the Navier–Stokes equations and equations for the energy balance, species concentration, equation of state and appropriate reaction rate relations.[25] We model the effects of turbulence with the k–ε model and the EDC model based on global reaction mechanisms.

2.1. The flow modelling

Let ρ and p denote the time averaged density and pressure, respectively. U_j is the Favre (density weighted) averaged velocity components in the (Cartesian) x_j directions. The averaged Navier–Stokes equations can be written as

$$\frac{\partial \rho}{\partial t}+\frac{\partial \rho U_j}{\partial x_j}=0, \tag{1}$$

$$\frac{\partial \rho U_i}{\partial t}+\frac{\partial \rho U_i U_j}{\partial x_j}=-\frac{\partial p}{\partial x_i}+\frac{\partial \tau_{ij}}{\partial x_j}+\frac{\partial}{\partial x_j}\left[\mu\left(\frac{\partial U_i}{\partial x_j}+\frac{\partial U_j}{\partial x_i}-\frac{2}{3}\delta_{ij}\frac{\partial U_l}{\partial x_l}\right)\right], \tag{2}$$

where μ is the molecular viscosity (to be taken as a function of the temperature), $\tau_{ij}=-\overline{\rho u_i u_j}$ is the Reynolds stress tensor, which is modelled as[12]

$$\overline{\rho u_i u_j}=\frac{2}{3}\delta_{ij}\left(\rho k+\mu_t\frac{\partial U_l}{\partial x_l}\right)-\mu_t\left(\frac{\partial U_i}{\partial x_j}+\frac{\partial U_j}{\partial x_l}\right). \tag{3}$$

k is the turbulent kinetic energy and μ_t is the so-called turbulent eddy viscosity computed from the k–ε model:

$$\mu_t=\rho C_\mu\frac{k^2}{\varepsilon}. \tag{4}$$

The governing equations for the turbulent kinetic energy, k, and its dissipation rate, ε, are given by

$$\frac{\partial \rho k}{\partial t}+\frac{\partial \rho k U_j}{\partial x_j}=\frac{\partial}{\partial x_j}\left[\left(\frac{\mu+\mu_t}{\sigma_k}\right)\frac{\partial k}{\partial x_j}\right]+S_k, \tag{5}$$

$$\frac{\partial \rho \varepsilon}{\partial t}+\frac{\partial \rho \varepsilon U_j}{\partial x_j}=\frac{\partial}{\partial x_j}\left[\left(\frac{\mu+\mu_t}{\sigma_\varepsilon}\right)\frac{\partial \varepsilon}{\partial x_j}\right]+S_\varepsilon. \tag{6}$$

Note that the effect of fluid compressibility in the k–ε model is accounted for through the following terms:

$$S_k=\tau_{ij}\frac{\partial U_i}{\partial x_j}-\rho\varepsilon-\frac{\mu_t}{\rho^2}\frac{\partial \rho}{\partial x_j}\frac{\partial p}{\partial x_j}, \tag{7}$$

$$S_\varepsilon=C_1\frac{\varepsilon}{k}\left[\tau_{ij}\frac{\partial U_i}{\partial x_j}-\frac{\mu_t}{\rho^2}\frac{\partial \rho}{\partial x_j}\frac{\partial p}{\partial x_j}\right]-C_2\rho\frac{\varepsilon^2}{k}. \tag{8}$$

In the relations above, density is linked with both pressure and temperature (T) through the equation of state:

$$p=\sum_a\frac{m_a}{W_a}R\rho T, \tag{9}$$

where R, m_a and W_a are the gas constant, the mass fraction and molecular weight of species a, respectively. The temperature is obtained from the energy equation:

$$\frac{\partial \rho h}{\partial t}+\frac{\partial \rho h U_j}{\partial x_j}-\frac{\partial p}{\partial t}=\frac{\partial}{\partial x_j}\left[\left(\frac{\mu+\mu_t}{\sigma_h}\right)\frac{\partial h}{\partial x_j}\right]+H_a^0 R_a, \tag{10}$$

where H_a^0 is the energy formation and $h=\int_{T_0}^{T}C_p\mathrm{d}T$ is the enthalpy. The equations for the mass

fractions, m_a, are modelled by

$$\frac{\partial \rho m_a}{\partial t}+\frac{\partial \rho m_a U_j}{\partial x_j}=\frac{\partial}{\partial x_j}\left[\left(\frac{\mu+\mu_t}{\sigma_m}\right)\frac{\partial m_a}{\partial x_j}\right]-R_a. \tag{11}$$

R_a is the chemical reaction rate of species a, where a is either fuel, oxygen, nitrogen, or carbon dioxide, etc. In equations (4)–(11), C_μ, C_1, C_2, σ_k, σ_ε, σ_h, σ_m are model constants, which are set according to the recommended values as in References 12 and 26: $C_\mu=0{\cdot}09$, $C_1=1{\cdot}44$, $C_2=1{\cdot}92$, $\sigma_k=1{\cdot}0$, $\sigma_\varepsilon=1{\cdot}22$, $\sigma_h=0{\cdot}7$, $\sigma_m=0{\cdot}7$.

2.2. *Global reaction scheme: laminar flows*

In most cases, not all elementary reactions are equally important. By neglecting the least important elementary reaction steps and assuming that several other species are in equilibrium, the number of species that has to be considered can be considerably reduced. For hydrocarbon fuel C_nH_{2n+2}, Hautman *et al.*[9] suggest that the following species are the most important: C_nH_{2n+2}, C_2H_4, H_2, CO_2, CO, H_2O and air (O_2 23·3% and N_2 76·7% in mass fraction). They suggest using the following four-step reaction mechanism:

$$C_nH_{2n+2}\rightarrow\frac{n}{2}C_2H_4+H_2, \tag{12}$$

$$C_2H_4+(O_2+3{\cdot}76N_2)\rightarrow 2CO+2H_2+3{\cdot}76N_2, \tag{13}$$

$$CO+\tfrac{1}{2}(O_2+3{\cdot}76N_2)\rightarrow CO_2+1{\cdot}88N_2, \tag{14}$$

$$H_2+\tfrac{1}{2}(O_2+3{\cdot}76N_2)\rightarrow H_2O+1{\cdot}88N_2. \tag{15}$$

The laminar reaction rates R_a denoted by R_a^{A} (to be distinguished from R_a^{M}, the reaction rate in turbulent flows) can be calculated from

$$R_a^{\mathrm{A}}=A_a\rho^d m_{\mathrm{fuel}}^a m_{\mathrm{oxygen}}^b m_{\mathrm{products}}^c \exp\left(-\frac{E}{RT}\right), \tag{16}$$

where A_a, a, b, c, d are empirical constants and E is the activation energy. The values of these constants are given in Reference 9.

In this scheme, equation (11) has to be solved for C_nH_{2n+2}, O_2, H_2, C_2H_4 and CO mass concentrations. The remaining three species, CO_2, H_2O and N_2, mass concentrations are solved by algebraic relations, derived by conservation from relations (12)–(15):

$$\begin{aligned} m_{H_2O}&=a_1m_{H_2}+a_2m_{C_2H_4}+a_3m_{CO}+a_4m_{CO_2},\\ m_{N_2}&=b_1m_{CO}+b_2m_{CO_2}+b_3m_{H_2O}+b_4m_{O_2},\\ 1&=m_{H_2O}+m_{H_2}+m_{C_3H_8}+m_{C_2H_4}+m_{CO}+m_{CO_2}+m_{O_2}+m_{N_2}, \end{aligned} \tag{17}$$

where a_i and b_i are constants: $a_1=-9$, $a_2=0{\cdot}4285$, $a_3=0{\cdot}8571$, $a_4=0{\cdot}5454$, $b_1=1{\cdot}88$, $b_2=2{\cdot}3927$, $b_3=2{\cdot}9244$, $b_4=3{\cdot}2918$. As we will see in the following, the intermediate species concentrations of H_2, C_2H_4 and CO are sometimes small and may be neglected. By doing so, one ends up with the single-step reaction scheme. Hautman *et al.*[9] and Westbrook *et al.*[27] suggest the following scheme:

$$C_nH_{2n+2}+\tfrac{1}{2}(3n+1)(O_2+3{\cdot}76N_2)\rightarrow nCO_2+(n+1)H_2O+1{\cdot}88(3n+1)N_2. \tag{18}$$

In this case, only two species concentration equations given by (11) have to be solved, i.e. for C_nH_{2n+2} and O_2. The reaction rate R_a can also be calculated by relation (16). The concentrations

of CO_2, H_2O and N_2 are solved by algebraic relations, derived from (18) in a similar way as is done in equations (17).

In other cases, one may have to use a higher level of detail to be able to analyse certain properties of the reacting flow field. Such a situation occurs when NO_x formation is of interest. In such a situation, one has to solve for those species that participate in the slow NO_x reactions. Currently, we are working on extending the current model to a quasi-equilibrium one, where the faster reactions are assumed to be in equilibrium. The slower, NO_x related, reactions (like those in the Zeldovich mechanism), on the other hand, are computed using chemical kinetics.[28,29]

2.3. *Reaction rate models: turbulent flows*

For turbulent flows, the species concentration equations given by (11) have to be averaged, which requires the time average of the reaction rate R_a. It has been shown[3,8] that the averaging of expression (16) for R_a is not appropriate and other methods, like PDF methods, the flamelet method or an EDC-type method, have to be used.

2.3.1. Finite-reaction-rate models. We use a model based on the EDC,[15] which assumes that the chemistry is fast enough and thus the reaction rate depends on the turbulent mixing rate. That is, the turbulent reaction rate, R_a^{M}, is related to the turbulent time-scale (k/ε) by

$$R_a^{\mathrm{M}} = B_a \rho \min\left(m_{\mathrm{fuel}}, \frac{m_{\mathrm{oxygen}}}{r} \right) \frac{\varepsilon}{k}, \tag{19}$$

where r is the stoichiometric constant of the reaction and B_a is a model constant. Often, one determines B_a by matching the numerical solution to measured data. One of the aims of this work is to assess the sensitivity of the solution on B_a. Relation (19) can be used for both the four-step reaction schemes given by (12)–(15) and the one-step reaction scheme given by (18). These schemes are based on the assumption that the chemical reaction rates are limited only by turbulent mixing. However, in places where the temperature is low, the reaction rate R_a^{A} computed from (16) by using the Reynolds averaged quantities may be even smaller and may become the limiting factor for chemical reactions. Consequently, in the computations we use the following:[30]

$$R_a = \min(R_a^{\mathrm{A}}, R_a^{\mathrm{M}}). \tag{20}$$

2.3.2. Infinite-reaction-rate: diffusion-flame model. For the single-step reaction scheme given by (18) and the diffusion-flame situation, when the reaction is very fast, one may use a simplified approach. That is, one assumes that fuel and air enter the combustion chamber through different inlet streams and react as they get in contact with each other. Since the model is simple, it has been used for a rather long time.[3,12]

Introduce a new variable q:

$$q = m_{\mathrm{fuel}} - \frac{m_{\mathrm{oxygen}}}{r}, \tag{21}$$

where r is the same as in (19). Definition (21) may be normalized to define the 'mixture fraction', f:

$$f = \frac{q - q_{\mathrm{oxygeninlet}}}{q_{\mathrm{fuelinlet}} - q_{\mathrm{oxygeninlet}}}. \tag{22}$$

Here, the subscripts oxygeninlet and fuelinlet denote the oxygen-supply and the fuel-supply inlets, respectively. Since $0 \leq m_a \leq 1$, $0 \leq f \leq 1$, equation (11) can be reduced by using $R_{\mathrm{oxygen}} = rR_{\mathrm{fuel}}$, to

a single equation for f:

$$\frac{\partial \rho f}{dt}+\frac{\partial \rho f U_j}{\partial x_j}=\frac{\partial}{\partial x_j}\left[\left(\frac{\mu+\mu_t}{\sigma_m}\right)\frac{\partial f}{\partial x_j}\right]. \tag{23}$$

Note that in (23) there are no source terms involved. For a given f, the mass fractions m_a can be computed in the following way. Let

$$f_s=\frac{-q_{\text{oxygeninlet}}}{q_{\text{fuelinlet}}-q_{\text{oxygeninlet}}}. \tag{24}$$

From (21) and (22), if $f<f_s$, i.e. $q<0$, then $m_{\text{fuel}}<m_{\text{oxygen}}/r$. The fuel will be consumed thoroughly, i.e. $m_{\text{fuel}}=0$, $m_{\text{oxygen}}=-rq$. In the case of fuel excess ($f>f_s$), the opposite situation occurs. Therefore, we have

$$f\leq f_s: \quad m_{\text{fuel}}=0, \qquad m_{\text{oxygen}}=-rq, \tag{25}$$

$$f>f_s: \quad m_{\text{fuel}}=q, \qquad m_{\text{oxygen}}=0. \tag{26}$$

In both cases, the mass fraction of the products, which include three species, CO_2, H_2O and N_2, can be computed by

$$m_{\text{products}}=1-m_{\text{fuel}}-m_{\text{oxygen}}. \tag{27}$$

The concentrations of every species in the products can be computed as in the case of the finite-reaction-rate model as is described in Section 2.2 [e.g. equations (17)].

2.4. Boundary conditions

The following boundary conditions have been implemented:

inlet boundary

U_i, h, m_a, f, k, ε are specified according to a given distribution.

wall boundary

$U_i=0$, $\mathrm{d}f/\mathrm{d}n=\mathrm{d}h/\mathrm{d}n=\mathrm{d}m_a/\mathrm{d}n=0$, k, ε are computed by using the so-called 'wall function'[5-7] relations.

outlet boundary

$$\mathrm{d}^2U_i/\mathrm{d}n^2=\mathrm{d}^2f/\mathrm{d}n^2=\mathrm{d}^2m_a/\mathrm{d}n^2=\mathrm{d}^2h/\mathrm{d}n^2=\mathrm{d}^2k/\mathrm{d}n^2=\mathrm{d}^2\varepsilon/\mathrm{d}n^2=0,$$

where n is the direction normal to the boundary. For the existence of a solution, global mass conservation has to be satisfied:

$$\int_\sigma \rho U_j \mathrm{d}\sigma_j=0, \tag{28}$$

where σ is the boundary of the domain.

3. NUMERICAL SOLUTION PROCEDURE

The system of PDEs given by equations (1), (2), (5), (6), (10) and (11) is discretized by finite differences on a globally and possibly a sequence of locally refined grids. The discrete equations are solved by a relaxation method. To accelerate the convergence a MG method is used.

3.1. *The grid system*

The grid is rectangular and uniformly distributed in each of the three Cartesian co-ordinates. This enables the discretization in a very simple form, and hence reduces the requirement for computer storage and the number of operators for expressing the discrete equations. To resolve regions where more grids are needed, one or more locally refined grids can be added. A sketch of the global and local grids, for the furnace case described below, is shown in Figure 1. In order to define the shape of the inlet more precisely, two additional levels of local grids are used. The merits of local grid refinements will be discussed and illustrated further below.

3.2. *The discretization scheme*

The discretization is done on a staggered grid. The spatial derivatives are discretized in the following way; all terms, with the possible exception of the convective terms, are approximated by central differences. The convective terms in all the equations are discretized by the hybrid scheme: central differences are used if the local Peclet number is less than 2; otherwise upwind differences are used.

When only steady state is sought, as in the cases considered here, one may use a quasi-time marching technique for the relaxation of the equation. By analogy to a time-dependent term we define a 'correction' term:

$$\frac{\partial \phi}{\partial t} \approx \frac{\phi^{n+1} - \phi^n}{\Delta t} \approx \beta \frac{U}{\Delta x} \Delta \phi. \tag{29}$$

The superscript n represents a pseudo-time-step, while $\Delta\phi$ represents the correction during each iteration. U is the characteristic velocity (usually taken as the maximum of the inlets velocities), Δx is the characteristic spatial mesh size and $\beta \geq 0$ acts as a scaling parameter. Usually, the smaller the values of β, the faster the convergence. However, occasionally when β is too small, the relaxation process may diverge.

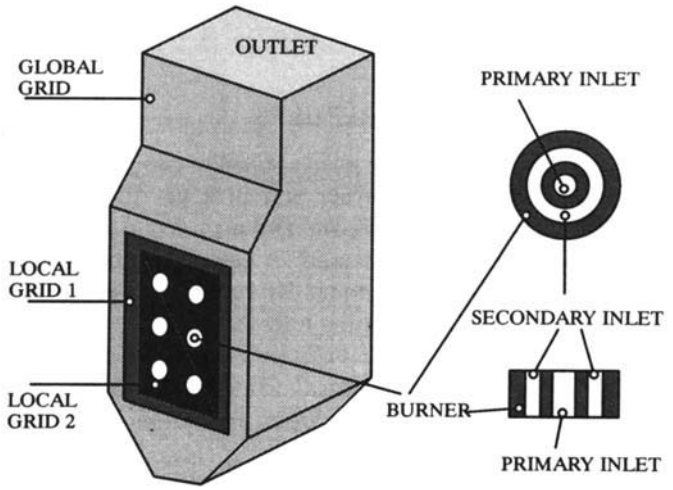

Figure 1. The six-burner furnace with its local grids. The geometry of each of the burners is shown enlarged.

3.3. *Solution of the discretized equations*

The initial field is assigned as follows:

$$(\rho, T, h, k, \varepsilon, m_a) = (\rho, T, h, k, \varepsilon, m_a)_{\text{inlet}},$$

$$(p, U_j, f) = \mathbf{0}.$$

The system of equations is relaxed in groups as follows:

(a) U_j, p,
(b) $k, \varepsilon, \mu_{\text{eff}}$,
(c) h, m_a, f

and, finally, updating

(d) ρ, μ.

This procedure is repeated until the iterations process converges. In step (a) the coupling of U_j and p is handled by a distributive Gauss–Seidel relaxation (cf. References 21 and 22 for more details). In the calculation of steps (a), (b) and (c) the relaxation is pointwise and lexicographically symmetric.

3.4. *Multi-grid acceleration*

The pointwise relaxation is simple but slow. In order to accelerate the convergence, a MG method is used. The solution procedure starts on a global grid doing several V-cycle MG relaxations in the fully approximate storage (FAS) mode.[21,22] After converging to a certain level, the variables are transferred to a finer local grid. The local grid is integrated into the MG V-cycling. This procedure is repeated until the finest local grid is introduced.

Restriction of scalars is done by volume averaging, and for the components of the velocity by area (flux conserving) averaging. Mass flux conserving restriction is a necessary condition for coarse grid convergence. This can be done by applying a conventional area restriction on the mass fluxes $\rho\mathbf{U}$($\mathbf{U}$ is the velocity vector). The corrections are interpolated to finer grids ('prolongated') by trilinear interpolations.

The MG procedure mentioned above has been found to be rather efficient for isothermal flows.[22,23]

4. RESULTS

The numerical methods described above have been applied to computing turbulent reacting flows in a combustion chamber with a single burner and in a gas fired furnace with six burners (Figure 1). The former case with separate propane and air inlets is used as a test bed for model parameter studies. The same geometry is also used for calculating the field corresponding to the infinitely fast reaction-rate (diffusion-flame) model. By varying one parameter at a time, we carry out several 'sensitivity' studies, that is, estimating how the calculated results vary with respect to numerical and model parameters: (i) numerical efficiency and accuracy (grid resolution dependence, Section 4.2); (ii) sensitivity to the numerical value of the EDC model parameter value (Section 4.3); (iii) sensitivity of the numerical solution to the particular chemistry model (Section 4.4).

Further details of the computed results for the single burner (Section 4.1) and the furnace case (Section 4.5) are given below.

4.1. Single burner

In Sections 4.1–4.4, we report calculation of reacting flows due to a single burner placed in a box with dimensions of $1 \times 1 \times 10$ units for width (W) × height (H) × length (L). The Reynolds number, based on the inlet flow and the inlet size, is 37 000. We have used $82 \times 50 \times 50$ grid points, which are expanded into four MG levels. The inlet flow temperature is 300 K. The propane–air mixture ratio is 3·9 : 100. The primary inlet velocity profile is uniform: 0·062 m/s. The secondary inlet velocity (uniformly distributed) is 0·676 m/s. The value of B_a in these calculations is set to 4. Figure 2 shows the mole fractions of species C_3H_8, H_2, O_2 and H_2O along spanwise direction for different streamwise sections, where X is the distance from the inlet and L is the total length of the box. Figure 3 shows the corresponding temperature profiles.

These figures depict a typical diffusion flame situation. Fuel and oxygen enter the combustor at different inlets marked by 'fuel' and 'air' in the figures. The surface (i.e. the flame front) where the fuel and oxygen meet is the reaction zone, provided that the local temperature is high enough. In the region where reaction occurs, the fuel and oxygen are consumed while intermediate species, such as H_2, are generated and transported downstream by advection and turbulent mixing. These intermediate products react also and are consumed successively, resulting in a thicker flame 'front'. Since the case calculated represents a lean fuel situation, one can note that with increasing distance from the burner O_2 is mixed with the products, leading to a decrease in the concentration of the products and a uniform distribution of O_2.

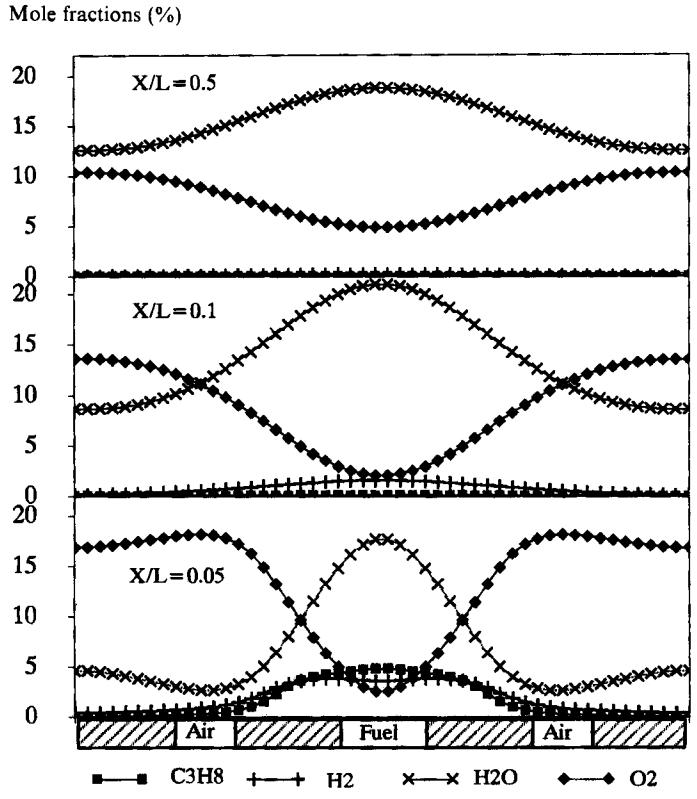

Figure 2. Mole fraction of C_3H_8, H_2 and H_2O in different downstream cross-sections

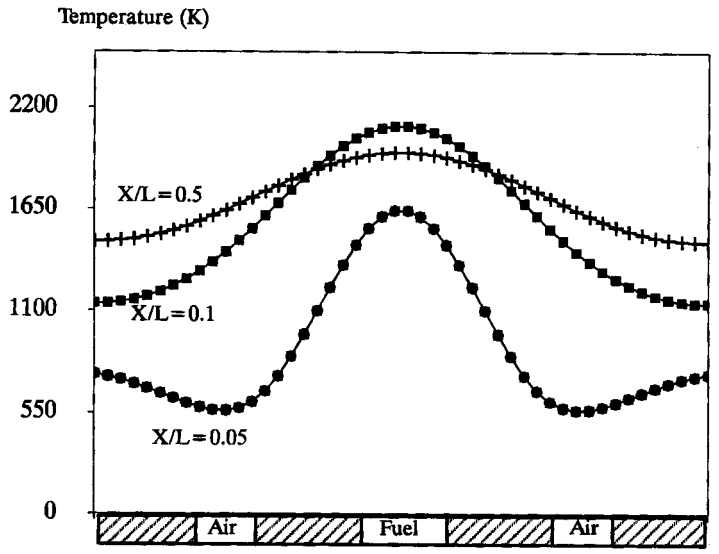

Figure 3. Temperature profiles at different planes parallel to the main flow direction

In this flame situation, single- and multiple-step finite-reaction-rate models and a single-step infinitely fast diffusion-flame model are all applicable, and are considered in the following. Before studying these models we examine the numerical efficiency of the solver.

4.2. Numerical efficiency and accuracy

The MG method and the local grid refinement technique have high numerical efficiency.[24] The efficiency of MG methods for non-reacting flows has been established previously.[22-24] For turbulent reacting flows, the situation is less established. Our experience with the MG solver for reacting flow situations is that the uncoupled (sequential) scheme that is described in Section 3.3 is non-optimal, but still offers a considerable improvement over other single-grid methods. Figure 4 depicts a typical speed-up of the MG method compared to the single-grid version of the same code. The speed-up depends on the grid size. MG methods are considerably less sensitive to the mesh spacing of the finest grid. It is also clear that our 'sequential' approach is non-optimal, in the sense that the convergence rate is not grid-independent (i.e. more than logarithmically dependent on the grid size). Improved MG convergence rates could possibly be achieved by tighter coupling of the equations ('block' solvers) during the smoothing process. By 'block' solvers we mean both solving systems of equations for neighbouring points as well as using all the governing equations simultaneously.

One obvious advantage of using locally refined grids is the reduction in the total number of grid points compared to global grids. Secondly, local grid refinements can be done 'adaptively' (i.e. depending on the solution), by estimating the levels of truncation errors in approximating the governing equations and thus reducing the number of node points considerably, without a loss of accuracy.[24,31] Global, uniform grids could require by at least an order of magnitude more computational grid points. Using grid stretching alone may reduce the number of grid points, but we estimate that it would still require a considerably larger number of grid points than the number required by local grid refinement. Large variations in cell aspect ratio imply also, unless

one uses symmetrical, multi-directional block relaxations, a reduction in the convergence rate. Thus, local grid refinement offers not only a reduced number of unknowns but also enables faster convergence of the iteration procedure.

An important issue in any numerical solution is the absolute level of accuracy of the *solution*. This question is directly related to the spatial grid resolution (and the order of discrete approximation). The same geometry and flow conditions are used in all the following calculations. Three different (global) grids are used: (1) $30 \times 18 \times 18$ (using three MG levels), (2) $58 \times 34 \times 34$ and (3) $82 \times 50 \times 50$. We estimate the grid dependence by comparing the variation of some of the dependent variables (computed on different grids) along the centre-line of the burner. In these calculations, the four-step, finite-reaction-rate EDC model is used. Figures 5 and 6 show the variation of the temperature and the mole fractions of some of the species along the centre-line of the burner, respectively. As seen, the variation between the results on grid-1 and grid-2 is rather

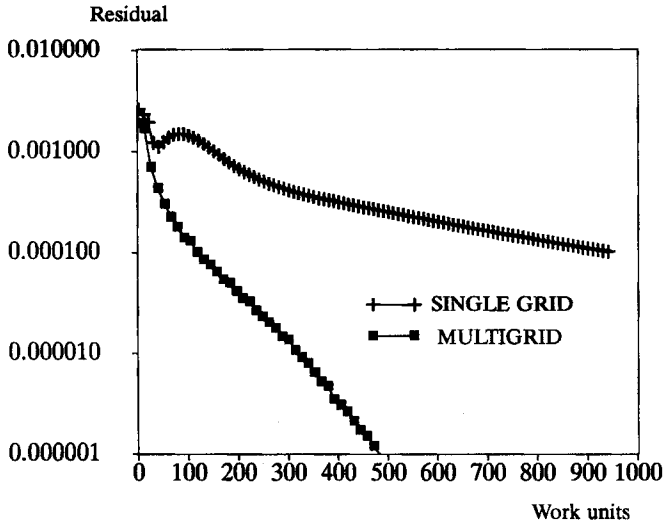

Figure 4. The convergence history of the residual in the continuity equation vs. the number of work units (equivalent to one relaxation sweep on the finest mesh); single- and multi-grid modes

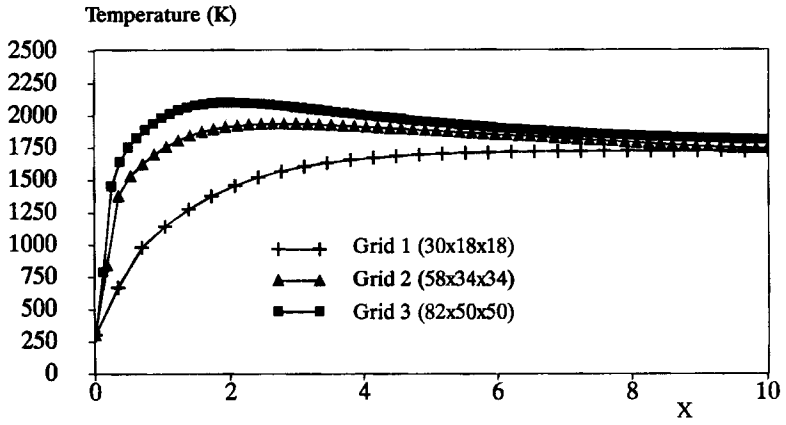

Figure 5. Temperature distribution along the axis of the burner, as calculated on different grids

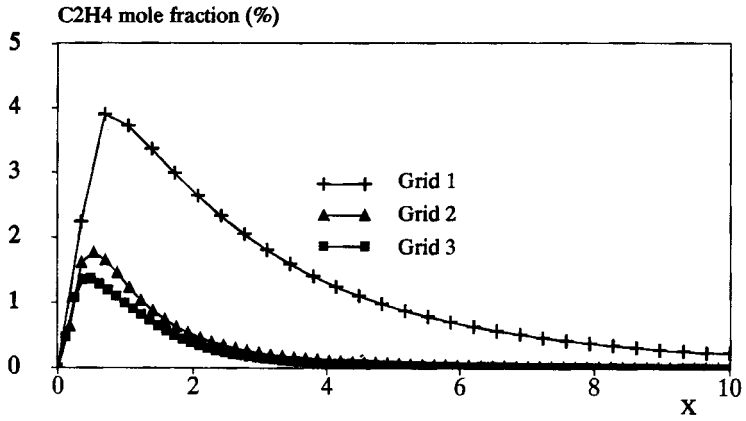

Figure 6(a). C_2H_4 distribution along the axis of the burner, as calculated on different grids

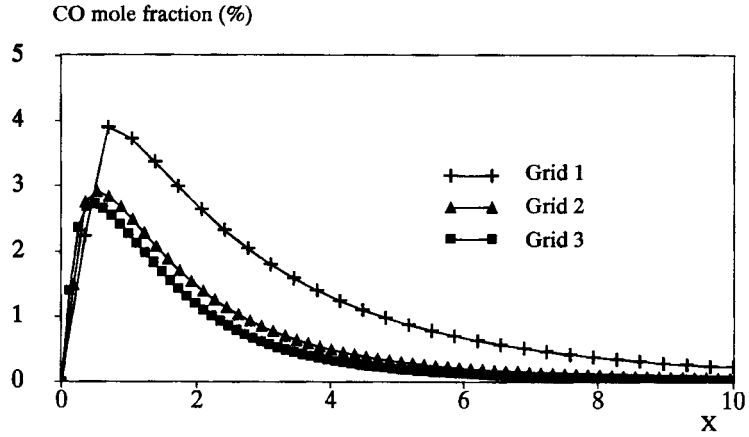

Figure 6(b). CO distribution along the axis of the burner as calculated on different grids

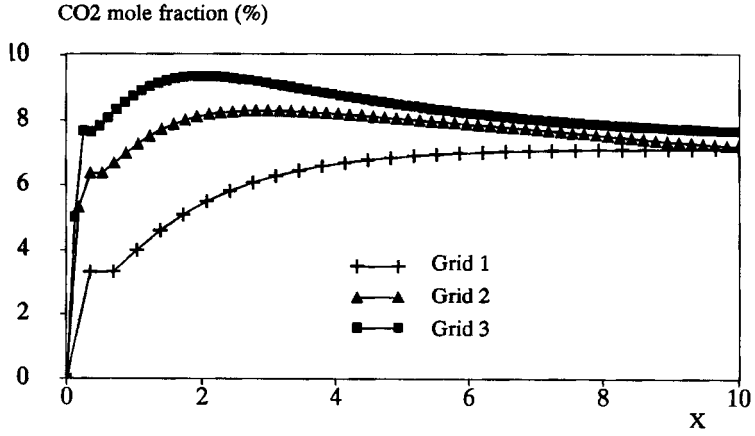

Figure 6(c). CO_2 distribution along the axis of the burner, as calculated on different grids

large, in particular for the concentrations of intermediate species (C_2H_4, CO, etc.). The change in the results as one moves from grid-2 to grid-3 is considerably smaller.

4.3. Sensitivity to chemistry model parameter

The four-step finite-rate chemistry model is used to consider the sensitivity of the solution to model parameter variations. The geometry is identical to the one described in Section 4.1, using a $58 \times 34 \times 34$ grid. The base values in the EDC models are those recommended by Magnussen *et al.*[15] [$B_a = 4$ in (19)]. Three different cases have been considered: $B = 2$, 4 and 6. For all species a, we take $B_a = B$. The larger the B, the faster the reaction rate. Figures 7 and 8 show the temperature and species mole fraction for the three values of B_a. The temperature distribution along the axis reaches the highest values closer to the inlet with increasing values of B. However, for low values of B (e.g. $B < 2$) the chemical process is relatively slow and it is incomplete, resulting in a lower peak temperature. The distribution of the CO_2 mass fraction follows that of the temperature, as expected. Also, larger values of B imply that the fuel and oxygen consumption is faster (Figure 8). From these figures one may note that the fuel and the intermediate species are not very sensitive to the value of B. On the other hand, CO_2, H_2O, O_2 and the temperature profiles are rather sensitive to B. This may imply that the EDC model is not robust, since B may depend on the particular flame situation and the fuel type itself.

4.4. Sensitivity to different reaction rate models

The comparison between the finite-reaction-rate model and the infinitely fast diffusion-flame model is carried out using the same single-burner combustor. Numerical solutions have been computed on a $58 \times 34 \times 34$ grid, using three different models. The three models, the infinitely fast diffusion-flame model, the one-step and the four-step finite-reaction-rate models, are studied using the EDC model parameter $B_a = 4$. Figures 9 and 10 show the temperature and some species mole fractions along the centre-line. One can note that the heat release rates are different with different models. The heat release rate of the single-step model is faster than that of the four-step finite-reaction-rate model. This can be explained by the fact that the existence of C_2H_4, CO and H_2 results in lower temperature, higher O_2 concentration and lower CO_2 and H_2O concentrations, compared with the results obtained from the one-step reaction scheme. This is qualitatively

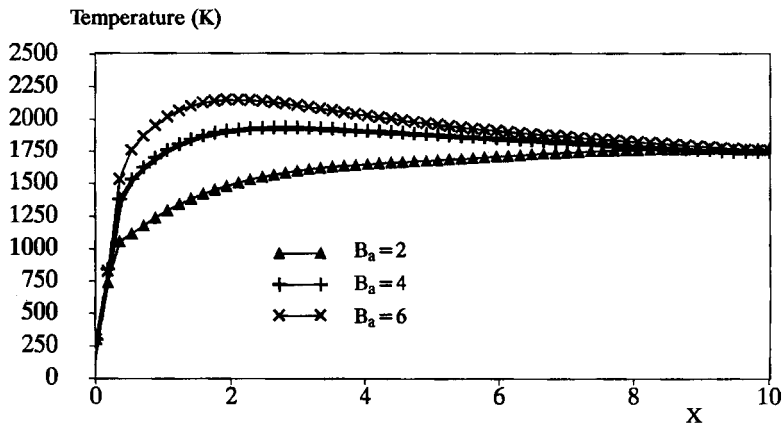

Figure 7. Temperature distribution along the axis of the burner for three different values of B: $B = 2$, 4 and 6

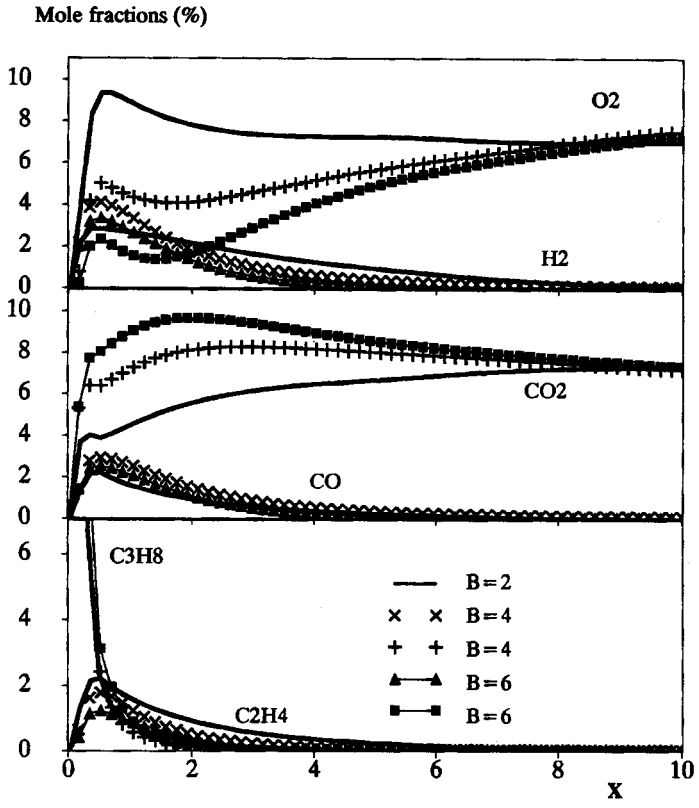

Figure 8. Mole-fractions distribution along the axis of the burner for three different values of B: $B=2$, 4 and 6

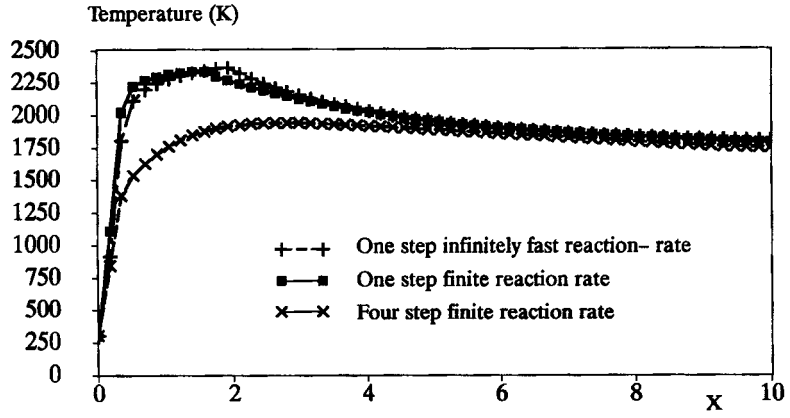

Figure 9. Temperature distribution along the axis of the burner for infinite-reaction-rate, single- and four-step finite-reaction-rate models

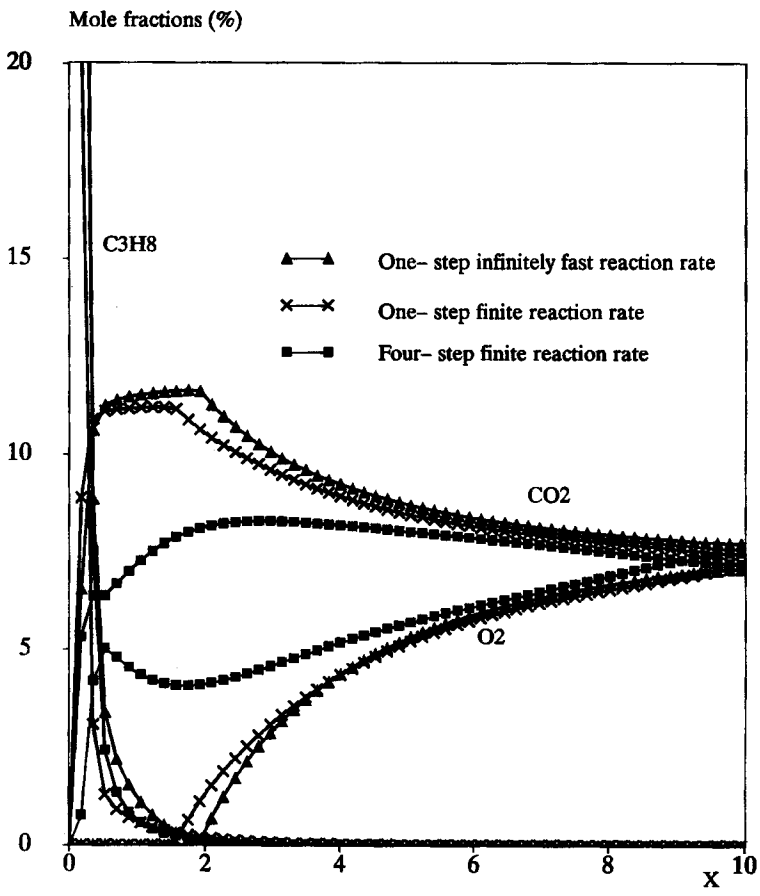

Figure 10. Mass-fraction distribution along the axis of the burner for infinite-reaction-rate, single- and four-step finite-reaction-rate models

in agreement with the experimental observations.[9-11] These effects may become important in certain situations. For short combustion chambers the difference between single-step and multiple-step reactions is more pronounced. Hence, the single-step reaction may be questionable in such situations. On the other hand, for well-stirred reactor situations, the results of the different models agree well with each other (cf. Figure 9 for $X > 5$). Figures 9 and 10 also show that both one-step finite-rate-reaction and infinitely fast diffusion-flame models are in rather good agreement with each other.

4.5. Six-burner-furnace flow

Finally, we illustrate the application of the reaction rate models to the simulation of the flow in a furnace, shown in Figure 1. As the problem is symmetric, we only compute half of the furnace. In general, turbulent reacting flows are rarely symmetric even though the geometry itself is symmetric. However, we solve for the averaged properties, and these quantities tend to be symmetric. The Reynolds number based on the inlet flow and the inlet size is $1{\cdot}3 \times 10^5$. If we would use a uniform grid with a resolution that is as fine as that for the previous single burner, the numerical

calculations would be more or less impossible, due to very long computational times and computer memory requirement. For this reason, we use a locally refined grid system to resolve the inlet region. The global grid is $66 \times 18 \times 30$, expanded into three MG levels and in addition two levels of locally refined grids, $52 \times 22 \times 16$ and $90 \times 26 \times 18$, placed around the inlet region are used. In each of the burners, propane is injected through the primary inlet at a speed of 1·684 m/s. The air is injected through the secondary inlet at a speed of 3·047 m/s. The swirl number for the fuel and the air streams is 0 and 0·3, respectively. The infinite-reaction-rate, (diffusion-flame) model is used in the following calculations.

Figure 11 shows the velocity vectors in a plane cutting through the burners. In the figure one may notice the extent of the locally refined grids. Figure 11(b) is a top view of the inlet region

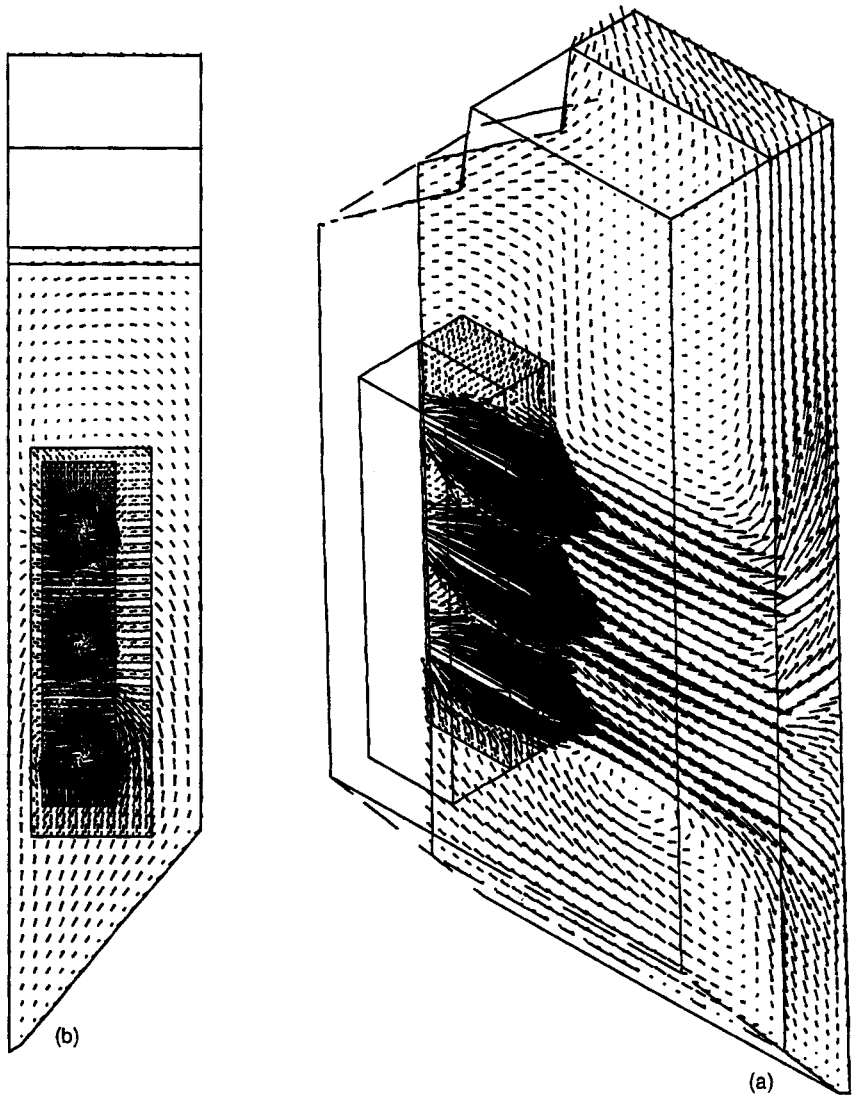

Figure 11. Velocity vectors in the six-burner furnace [Figure 11(a)]. Note the locally refined grids near the burners. Top view of the inlet region [Figure 11(b)]

demonstrating the grid resolution effects. As seen with local grids the inlet shape is described more accurately, which is important for getting the correct mass and momentum fluxes at the inlets. Also, the swirling motion generated by the burners is seen clearly. Figure 12 shows the corresponding mixture fraction field. Line J ($f \approx 0{\cdot}06 \approx f_s$) around the three inlets is the location where the fuel and the oxygen are at stoichiometric ratio, leading to a complete combustion. The mass fraction of the fuel and oxygen are all zero while CO_2 and H_2O reach their maximum values. Between line J and the inlets are the regions where $f > f_s$. The fuel is entering through these regions and therefore the fuel is in access and the O_2 mass fraction vanishes. Lines A to J, located outside the fuel-rich region, have mixture fraction values which are less than the stoichiometric value (f_s). This means that the region is O_2-rich and the mass fraction of the fuel is zero.

Figure 13 depicts the temperature field. One can observe that the location corresponding to line J in Figure 12, denoting the flame-front location, has the peak temperature (2200 K). In the fuel-rich regions the temperature is low because the fuel is cold when entering the furnace, and is being heated up as it gets closer to the flame front. In the O_2-rich region, the cold air (from the inlets) has a cooling effect on the hot gas, so the temperature decreases in these regions. The figure also shows that the outlet temperature is considerably lower (by about 900 °C) than the maximal value inside the furnace. It should be pointed out that in these calculations we have not included heat-radiation effects. Our previous experience in calculating flows with and without heat radiation is that the large temperature difference noted above would be considerably reduced once radiation is taken into account.

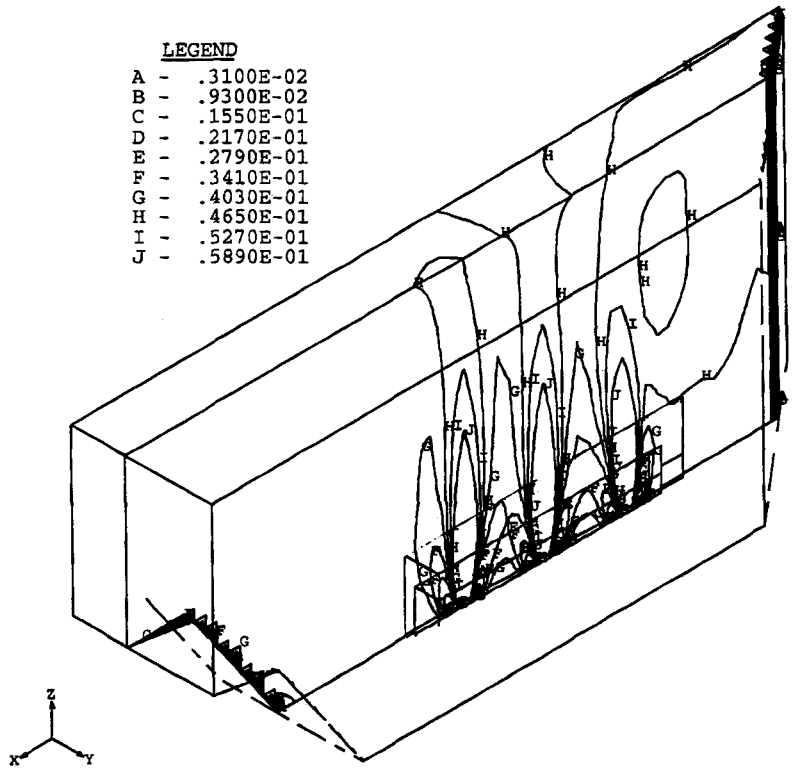

Figure 12. Mixture fraction field in the six-burner furnace, using the infinite-reaction-rate model. The flame front is marked by line J

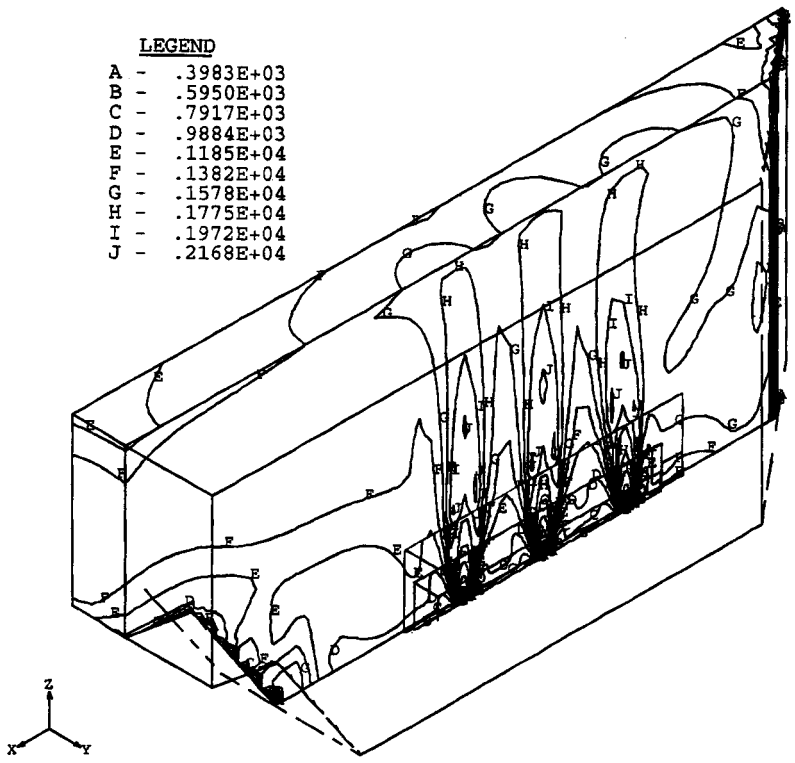

Figure 13. Isotherms in the six-burner furnace, using the infinite-reaction-rate model

5. DISCUSSION AND CONCLUDING REMARKS

Numerical modelling of turbulent reacting flows requires the introduction of models for turbulence, its interaction with species mixing and the chemical reactions. All these models introduce new parameters which have to be determined empirically (i.e. 'model calibration'). An essential prerequisite for model calibration and validation is a knowledge of the accuracy of the numerical results in solving the governing equations. Here, we have studied the accuracy and efficiency of the numerical results. It has been shown that good numerical efficiency can be achieved by the MG solver. Further, the spatial resolution can be increased in a rather simple manner by local grid refinements. An examination of different chemical reaction models shows that multiple-step reaction models not only give important information on intermediate chemical species, such as CO, H_2, NO_x, etc., but also result in a more realistic flame speed. In some well-conditioned combustors and where the reactions are fast enough, one may use simpler models (i.e. a single-step reaction model). The species concentrations and the temperature field are sensitive to the value of the EDC model parameter at the flame-front region. Not too close to the flame front, the dependence on the model parameter is considerably less pronounced. This behaviour opens the possibility of using the EDC model for engineering applications when the detailed temperature distribution is of minor interest. In other situations one should consider the impact of the basic assumptions behind the EDC model, especially for multiple-step reactions, where B_a may not be assumed to be equal for all the different reaction steps.

ACKNOWLEDGEMENT

This work was supported by NUTEK (The Swedish Board for Technical Development) under contract 91-56606P.

REFERENCES

1. P. A. Libby and F. A. Williams, 'Some implications of recent theoretical studies in turbulent combustions', *AIAA J.*, **19,** 261–274 (1981).
2. S. B. Pope, 'Turbulent premixed flames', *Ann. Rev. Fluid Mech.*, **19,** 237–270 (1987).
3. R. Borghi, 'Turbulent combustion modelling', *Prog. Energy Combust. Sci.*, **14,** 245–292 (1989).
4. P. Hutchinson, E. E. Khalil and J. H. Whitelaw, 'Measurement and calculation of furnace flow properties', *J. Energy*, **1,** 212–219 (1977).
5. C. G. Speziale, 'Discussion of turbulence modeling: past and future', *NASA CR 181884*, 1989.
6. B. E. Launder and D. B. Spalding, 'The numerical computation of turbulent flows', *Comput. methods appl. mech. eng.*, **3,** 269–289 (1974).
7. W. Rodi, 'Turbulence models and their application in hydraulics—a state of the art review', Institut for Hydromechanik, 1980.
8. P. Givi, 'Model-free simulations of turbulent reactive flows', *Prog. Energy Combust. Sci.*, **14,** 1–107 (1989).
9. D. J. Hautman, F. L. Dryer, K. P. Schug and I. Glassman, 'A multiple-step overall kinetic mechanism for oxidation of hydrocarbons', *Combust. Sci. Technol.*, **25,** 219–235 (1981).
10. C. K. Westbrook and F. L. Dryer, 'Chemical kinetics and modeling of combustion process', *Proc. 18th Int. Symp. on Combustion*, The Combustion Institute, Pittsburgh, 1981, p. 749.
11. W. P. Jones and R. P. Lindstedt, 'Global reaction schemes for hydrocarbon combustion', *Combust. Flame*, **73,** 233–249 (1988).
12. W. P. Jones and J. H. Whitelaw, 'Calculation methods for reacting turbulent flows: a review', *Combust. Flame*, **48,** 1–26 (1982).
13. P. A. Libby and F. A. Williams, 'Turbulent reacting flows', in *Topics in Applied Physics*, Vol. 44, Springer, Berlin, 1980.
14. D. B. Spalding, 'Development of the eddy break-up model of turbulent combustion', *Proc. 16th Int. Symp. on Combustion*, The Combustion Institute, Pittsburgh, 1976, p. 1657.
15. B. F. Magnussen and B. H. Hjertager, 'On mathematical modelling of turbulent combustion with special emphasis on soot formation and combustion', *Proc. 16th Int. Symp. on Combustion*, The Combustion Institute, Pittsburgh, 1976, pp. 719–729.
16. S. B. Pope, 'Computations of turbulent combustion: progress and challenges', *Proc. 23rd Int. Symp. on Combustion.* The Combustion Institute, Pittsburgh, 1990, pp. 591–612.
17. J.-Y. Chen and W. Kollman, 'Chemical models for pdf modelling of hydrogen–air nonpremixed turbulent flames', *Combust. Flame.* **79,** 75 (1990).
18. N. Peters, 'Laminar diffusion flamelet models in non-premixed turbulent combustion', *Prog. Energy Combust. Sci.*, **10,** 319–339 (1984).
19. F. C. Lockwood, C. Papadopoulos and A. S. Abbas, 'Prediction of a corner-fired power station combustor', *Combust. Sci. Technol.*, **58,** 5–23 (1988).
20. D. Wennerberg, 'Prediction of pulverized coal and peat flames', *Combust. Sci. Technol.*, **58,** 25–41 (1988).
21. A. Brandt, 'Multi-level adaptive solution to boundary-value problem', *Math. Comput.*, **31,** 333–390 (1977).
22. L. Fuchs, and H. S. Zhao, 'Solution of three-dimensional viscous incompressible flows by a multi-grid method', *Int. j. numer. methods fluids*, **4,** 539–555 (1984).
23. X. S. Bai and L. Fuchs, 'A fast multi-grid method for 3-D turbulent incompressible flows', *Int. J. Numer. Method Heat Fluid Flows*, **2,** 127–137 (1992).
24. L. Fuchs, 'A local mesh refinement technique for incompressible flows', *Comput. Fluids.* **14,** 69–81 (1986).
25. F. A. Williams, 'Turbulent combustion', in J. D. Buckmaster (ed.), *The Mathematics of Combustion*, Chap. 3, SIAM, Philadelphia, 1985.
26. E. E. Khalil, *Modelling of Furnaces and Combustors*, Abacus Press, Tunbridge Wells, 1982.
27. C. K. Westbrook and F. L. Dryer, 'Simplified reaction mechanisms for the oxidation of hydrocarbon fuels in flames', *Combust. Sci. Technol.*, **27,** 31–43 (1981).
28. J. A. Miller and C. T. Bowman, 'Mechanism and modeling of nitrogen chemistry in combustion', *Prog. Energy Combust. Sci.*, **15,** 287–338 (1989).
29. M. C. Drake and R. J. Blint, 'Calculation of NO_x formation pathways in propagating laminar, high pressure premixed CH_4/air flames', *Combust. Sci. Technol.*, **75,** 261–285 (1991).
30. C. S. Lin, 'Numerical calculation of turbulent reacting flow in a gas-turbine combustor', *NASA TM 89842*, 1987.
31. X.-S. Bai and L. Fuchs, 'Turbulent reacting flows past bluff bodies: assessment of accuracy and efficiency' *Computers and Fluids*, (1993) (to appear).